Mixed Analytical/Numerical-Spectral Element Algorithm for Efficient Solution of Problems with Interior or Boundary Layers

U. Zrahia*   S. A. Orszag†   M. Israeli‡

Abstract

An efficient high-order solution for a boundary and interior layer problem which is applicable to multi-dimensional problems is presented. The solution is a combination of a global penalty spectral element solution obtained on a coarse grid and a local one dimensional analytical approximation. The solution is further improved numerically on a coarse grid. Results for interior and boundary layer problems are presented.

Key words: spectral-element, asymptotic methods, penalty method, boundary layer, interior layer.

AMS subject classifications: 65N30, 35J25.

1   Introduction

Singular perturbation problems arise in many problems, including solid mechanics, fluid flow, heat transfer and semiconductor devices ([1],[2],[3]), when the highest derivative in the differential equation under consideration is multiplied by a small parameter ϵ. The solution to such problem exhibits a boundary layer within the domain with a characteristic width which is a function of the small parameter ϵ. Solutions for this type of problem can be obtained by numerical methods, asymptotic techniques [4] or mixed methods [10] which are based on a combination of numerical and asymptotic solutions. However, numerical solution of a singular perturbation problem is increasingly difficult as ϵ becomes smaller. Indeed, a large number of grid points

*Fluid Dynamics Research Center, Princeton University Princeton, NJ 08544-0710, U.S.A.

†Fluid Dynamics Research Center, Princeton University Princeton, NJ 08544-0710, U.S.A.

‡Computer Science Department, Technion, Israel Institute of Technology, Haifa 32000, Israel

are required to resolve the boundary layer if $\epsilon \ll 1$. In order to overcome this difficulty an adaptive mesh combined with non-conforming meshes can be used([5], [6], [4]). High order numerical solutions can be obtained, e.g., by 'mortar spectral elements' ([7], [8]). Asymptotics is useful if it is possible to expand the solution in terms of the small parameter ϵ. For singular perturbation problems the asymptotic solution is usually composed of an inner solution, u_i, which is valid in the neighborhood of the boundary layer and an outer solution, u_o, which is valid far from the boundary layer. The accuracy of the asymptotic approximation is of $O(\epsilon^{j+1})$, where ϵ is the small parameter and j is the order of the asymptotic expansion. Flaherty and O'Malley [9] developed an algorithm which solves numerically for the inner and outer asymptotic solutions using a standard numerical method. On the other hand, the 'booster method' [10] combines an asymptotic solution of $O(\epsilon^{j+1})$ [9] with known discretization methods. An improvement of the numerical solution by factor of $O(\epsilon^{j+1})$ can be obtained. An implementation of the method for finite elements (ASFE) was done in [11]. This approach is difficult to implement for multidimensional problems with complex geometries, because an asymptotic solution is not always available to replace the analytical solution. A more accurate procedure, albeit much more expensive one, is to replace the asymptotic inner solution by a multidimensional numerical inner solution [12].

Here we present an alternative way to obtain efficient solutions for boundary and interior layer problems which is applicable to d-dimensional problems with $d \geq 1$. An approximate solution, u_A, which is constructed by an inner and an outer solution, is calculated. The outer solution, u_o, which is valid far from the boundary layer, is a function of $\mathbf{x} \in \Omega \subset \mathcal{R}^{\mathbf{d}}$. It is calculated numerically within the domain on a coarse mesh (Sec. 3). The inner solution, u_i, which is valid in the neighborhood of the boundary layer, is assumed to be a function of $x \in \Omega \subset \mathcal{R}^1$ (Sec. 4). The solution for u_A is computationally low-cost both because its outer component is calculated numerically on a coarse grid and because its inner component is defined on a one-dimensional domain and calculated analytically. This

solution is used as a first approximation and is improved by solving a modified equation numerically on the same coarse grid as for the outer solution (Sec. 5), yielding an accurate composite solution to the problem.

2 Overview of the method of solution

Let us consider a boundary value problem for the partial differential equation:

$$(1) \qquad \epsilon \nabla^2 u + \mathbf{V} \cdot \nabla u + au = f$$

where $u, f, \mathbf{V}$, are functions of $\mathbf{x} \in \Omega \subset \mathcal{R}^{\mathbf{d}}$, d is the number of space dimensions, ϵ is a small positive parameter and a is assumed to be negative. We further assume that u is twice differentiable while $f(\mathbf{x})$ may have a finite number of jump discontinuities.

Let Γ_b be the part of the boundary, $\Gamma \equiv \partial \Omega$, which supports a boundary layer, and let Γ_g be the complement of Γ_b in Γ.

We assume that Dirichlet boundary conditions are imposed,

$$(2) \qquad \begin{array}{cccc} u & = & U_b & on & \Gamma_b \\ u & = & U_g & on & \Gamma_g \end{array}$$

and lead to a unique solution of the problem.

The solution of (1)-(2) may have two types of layers: interior or boundary layers. Boundary layers are located at boundaries of the domain (i.e. Γ_b). Their thickness and location depend on the angle between the characteristic curves of the reduced equation (obtained by setting ϵ to zero in (1)) and the boundary [1]. Interior layers appear at the interior discontinuities of $f(\mathbf{x})$ and preserve the smoothness of the solution at these locations.

Problem (1) has often been considered as a test case for different numerical schemes. It is known that most of numerical methods fail when the cell Reynolds number $\frac{v\Delta x}{\epsilon}$ becomes larger than $O(1)$. Here Δx is a typical length between two grid points and $v = \max_{\Omega(\mathbf{x})}(|V|)$.

In brief, the steps of our new algorithm are:

(i) The numerical solution of (1) on a fixed coarse grid is obtained with a special set of boundary conditions, to serve as an approximation for the outer solution, u_o (Sec. 3).

(ii) A set of one-dimensional boundary layer equations arising from (1) are solved on rays starting at each point of Γ_b, advancing along the inner normal at that point(Sec. 4).

(iii) The outer solution, u_o, and inner solution, u_i, are matched to obtain an approximate composite solution, u_A (Sec. 4).

(iv) Correction terms are computed and added to the right hand side of the discrete approximation of (1). The corrected discrete approximation is solved to obtain an improved solution , u_I (Sec. 5).

(v) Any discrepancy between the improved solution, u_I, and the approximate solution, u_A, is reduced by repeating steps (ii) to (v) (Sec. 6).

In section 7 we present numerical results for problems exhibiting interior or boundary layers.

3 Outer solution

The aim of the present section is to describe the calculation of our approximation to the outer solution u_o. The solution of (1), subjected to natural boundary conditions on Γ_b and to the original Dirichlet boundary conditions on Γ_g, is obtained numerically using a spectral method with polynomial basis of degree N in each of the d-space dimensions. The calculated solution, u_o, is smooth and converges to the exact solution far from the boundary layer when $N \rightarrow \infty$ for fixed ϵ.

A penalty spectral element formulation is used for the solution of u_o. The spectral element method [13] is chosen since the outer solution is expected to be smooth (without large gradient) and therefore this method can achieve an accurate solution with a minimal number of degrees of freedom. The Dirichlet boundary conditions on Γ_b are imposed as penalty terms. The reason for choosing a penalty method will be discussed below.

Applying the weighted residuals method followed by Green's theorem to (1)-(2) results in the following weak formulation for $u \in (H_E^1(\Omega))^d$:

$$
\begin{aligned}
& - \int\int_\Omega \epsilon \nabla w \nabla u d\Omega + \int\int_\Omega w(\mathbf{V}\nabla u)d\Omega + \\
& \qquad \int\int_\Omega awud\Omega + \oint_\Gamma \epsilon w \nabla u d\Gamma - \\
(3) \qquad & \int_{\Gamma_b} \epsilon w \nabla u d\Gamma_b + \lambda \int_{\Gamma_b} w(u - U_b)d\Gamma_b = \\
& \qquad\qquad \int_\Omega wfd\Omega \\
& \qquad\qquad \forall w \in (H_0^1(\Omega))^d
\end{aligned}
$$

In the above equation, $\lambda = 0$ yields natural boundary conditions on Γ_b while large λ forces essential (Dirichlet)

boundary conditions on Γ_b. The formulation (4) is applicable both to the outer solution, u_o, and to the improved solution, u_I (see Sec. 5). After discretization by the penalty spectral element approach, an approximate solution ,u^h, is sought such that:

$$\sum_{e=1}^{n}\{-\int\int_{\Omega^e}\epsilon\nabla w^h\nabla u^h d\Omega^e +$$

$$\int\int_{\Omega^e}w^h(\mathbf{V}\nabla u^h)d\Omega^e + \int\int_{\Omega^e}aw^h u^h d\Omega^e +$$

(4)
$$\oint_{\Gamma^e}\epsilon w^h\nabla u^h d\Gamma - \int_{\Gamma_b\cap\Omega^e}\epsilon w^h\nabla u^h d\Gamma +$$

$$\lambda\int_{\Gamma_b\cap\Omega^e}w^h(u^h - U_b)d\Gamma_b\} = \int_{\Omega}w^h f d\Omega$$

$$\forall w^h \in (H_0^1(\Omega^e))^d$$

where u^h is the approximate solution obtained by Lagrange interpolation of order N at the Gauss-Lobatto-Legendre points and n is the total number of elements. The integrations in (5) are performed by employing Gauss-Lobatto-Legendre quadrature leading to a set of algebraic equations.

The penalty method as presented here is more efficient for the numerical treatment of interior layers than is a standard spectral element method. In the latter case, additional assembly is required, while in the present approach the same spectral element matrices are needed for both the outer and the improved solutions. These matrices only differ by the terms which are multiplied by λ.

4   Inner solution

The outer solution is valid only far from Γ_b and thus should be corrected by an inner solution, u_i, which is valid near the boundary Γ_b. In order to investigate the solution in the neighborhood of Γ_b we first employ for the two-dimensional case a coordinates transformation $\mathbf{x} = (x, y) \to (\xi, \eta)$. For a point $\mathbf{x}$ close to Γ_b let us define a coordinate system (ξ, η) originating on the nearest point $\mathbf{x}_0$ on Γ_b to $\mathbf{x}$. Let η be the coordinate tangential to Γ_b and let ξ be the fast variable in the orthogonal direction of Γ_b normalized with respect to ϵ. The transformation $(\mathbf{x}) \to (\xi, \eta)$ for $\Omega \subset \mathcal{R}^2$ is given locally near Γ_b by:

(5)
$$\mathbf{x}(\xi, \eta) = \mathbf{x}_o + \xi\mathbf{n}$$

where $\mathbf{n} = [-\frac{\partial y_0}{\partial\eta}, \frac{\partial x_0}{\partial\eta}]$. The inner solution, u_i, is obtained by substituting the asymptotic expansion:

$$u_i(\xi; \epsilon) = \sum_{n=0}^{\infty}(u_i)_n\epsilon^n$$

into (1) and collecting the leading-order terms. Unless we encounter a corner region, we obtain a one-dimensional second-order differential equation with a local coordinate ξ.

The inner solution, u_i, satisfies the boundary conditions:

$$u_i(\xi = 0, \eta) = U_b(\eta) - u_o(\xi = 0, \eta)$$
$$u_i(\xi \to \infty, \eta) = 0$$

(6)
$$\forall\eta \in \Gamma_b$$

where the values for u_o are taken from the outer solution process which was obtained in Sec. 3.

These one-dimensional problems are defined for each η on the boundary. They are to be solved along rays orthogonal to the boundary Γ_b and originating at grid points lying on Γ_b.

The resulting inner solution gives the approximate solution:

(7)
$$u_A(\mathbf{x}; \epsilon) = u_o(\mathbf{x}) + u_i(\xi(\mathbf{x}), \eta(\mathbf{x}))$$

which is an $O(\epsilon)$ approximation through Ω.

For the two-dimensional case, the values of the outer solution are updated twice: first, after computation of the x-boundary layer, and then after computation of the y-boundary layer. This second update mostly affects the solution in the corner where the x and y boundary layers meet. The extension to three-dimensional problems is then straightforward. A more accurate procedure, albeit more expensive, is to use a two-dimensional inner solution in corners.

5   Improved solution

The 'booster method', introduced by Israeli and Ungarish ([10]), exploits analytic asymptotic approximations (or possibly other approximation methods) to obtain an accurate global approximation to the solution of a partial differential equation on a coarse grid. The method is summarized as follows:

For a linear partial differential equation:

(8)
$$L(u) = f \quad in \quad \Omega$$

subject to appropriate boundary conditions, a numerical solution u_n is usually obtained directly from:

(9)
$$L_h(u_n) = f_h \quad in \quad \Omega$$

where L_h and f_h are the discretized approximations for L and f. Instead, in the 'booster method', we use an approximate analytic solution, u_A of (8) to obtain an improved solution u_I from:

$$(10) \quad L_h(u_I) \quad = \quad L_h(u_A) - L(u_A) + f_h \qquad in \quad \Omega$$

The error of the improved solution obtained by the booster method is bounded by: $||e_I|| \leq k||e_n|| \cdot ||e_A||$ (see [10]).

Equation (10) can be used in order to improve both the approximate solution, u_A, which was calculated in Sec. 4 and a spectral element solution of (1)-(2).

6   Summary of the algorithm

6.1   Steps of the algorithm

The algorithm proposed here is summarized as follows:

1. The outer solution, u_0, to (1) is obtained numerically on a coarse grid using (5) and letting λ tend to zero.

2. The inner solution, u_i, is obtained analytically according to Sec. 4.

3. The two solutions, u_0 and u_i, are matched according to (16) to obtain an "analytic" approximation, u_A, to the exact solution(16).

4. Equation (10) is solved (on a coarse grid) using an appropriate choice for λ.

5. The outer part of u_I is substituted into u_A and step 2 is repeated until convergence is attained. The outer part of u_I is calculated by subtraction of u_i from u_I.

6.2   Interpolated solution

The numerical solution, $\mathbf{u}_I$, is a discrete solution calculated at the nodal points of the elemental grid. Intermediate values for the solution, $u_I(\mathbf{x})$, cannot be obtained by direct interpolation using the spectral element basis since the solution does not belong to the space spanned by this basis ([11]). An alternative procedure to calculate the value of $u_I(\mathbf{x})$ is as follows:

$$(11) \qquad \mathbf{K}\mathbf{u}_I = \mathbf{f} + (\mathbf{K}\mathbf{u}_A - \mathbf{f}^A)$$

or alternatively:

$$(12) \qquad \mathbf{K}(\mathbf{u}_I - \mathbf{u}_A + \mathbf{K}^{-1}\mathbf{f}^A) = \mathbf{f}$$

If we define:

$$(13) \qquad \mathbf{u}_m = (\mathbf{u}_I - \mathbf{u}_A + \mathbf{K}^{-1}\mathbf{f}^A)$$

then

$$(14) \qquad \mathbf{K}\mathbf{u}_m = \mathbf{f}$$

The function $u_m(\mathbf{x})$ satisfies (14) and thus, belongs to the space spanned by the spectral element basis. Therefore $u_m(\mathbf{x})$ can be expressed as:

$$(15) \qquad u_m(\mathbf{x}) \quad = \quad I_N(\mathbf{u}_m)$$

where I_N is the spectral-element interpolation operator based on Legendre-Gauss-Lobatto points. The analytical approximation is composed of the numerical outer solution, $\mathbf{u}_o$, and the analytical inner solution, $u_i(\xi(\mathbf{x})\eta(\mathbf{x})$, so that:

$$
\begin{aligned}
u_A(\mathbf{x}) \quad &= \quad u_o(\mathbf{x}) + u_i(\xi(\mathbf{x}), \eta(\mathbf{x})) \\
(16) \qquad &= \quad I_N(\mathbf{u}_o) + u_i(\xi(\mathbf{x}), \eta(\mathbf{x}))
\end{aligned}
$$

The inner solution, u_i, is analytical and continuous in $\xi(\mathbf{x})$ but it is discrete in $\eta(\mathbf{x})$. As a result we can write for each discrete point η_n an analytical solution $u_i(\xi, \eta_n)$. The inner solution at $\eta \neq \eta_n$ can be calculated by a one-dimensional Lagrange interpolation formula of order N. That is because of the restriction that the variation of the inner solution in the η direction is determined by the outer solution which is spanned by the spectral element basis.

If we introduce the booster term

$$(17) \qquad \mathbf{u}_r \quad = \quad \mathbf{K}^{-1}\mathbf{f}^A$$

with

$$(18) \qquad u_r(\mathbf{x}) \quad = \quad I_N(\mathbf{u}_r)$$

Then, the improved solution u_I is expressed as:

$$
\begin{aligned}
u_I(\mathbf{x}) \quad &= \quad I_N(\mathbf{u}_o) + u_i(\xi(\mathbf{x})) + I_N(\mathbf{K}^{-1}\mathbf{f}^A) \\
(19) \qquad &= \quad I_N(\mathbf{u}_o + \mathbf{K}^{-1}\mathbf{f}^A) + u_i(\xi(\mathbf{x}))
\end{aligned}
$$

7   Numerical results

7.1   Two-dimensional   problem   with   boundary layer

Here we apply the method described above to the two-dimensional convection-diffusion problem:

$$
\begin{aligned}
\epsilon\nabla^2 u + \mathbf{V} \cdot \nabla u \quad &= \quad 0 \qquad \mathbf{x} \in (0,1)^2 \\
u(x,0) \quad &= \quad 0 \\
u(x,1) \quad &= \quad \sqrt{x} \\
u(0,y) \quad &= \quad 0 \\
(20) \qquad u(1,y) \quad &= \quad \sqrt{y}
\end{aligned}
$$

where $\mathbf{V} = (1,1)$.

For this problem we seek an asymptotic solution composed of an outer solution. u_o, and an inner solution, u_i, as follows:

$$(21) \qquad u_A(\mathbf{x}; \epsilon) \;=\; u_o(\mathbf{x}) + \sum_{n=0}^{\infty} (u_i)_n \epsilon^n$$

The solution for u_o is two-dimensional and is computed as described in Sec. 3. For the inner solution (setting $n = 0$ in (21)) the following one-dimensional differential equation must be solved in the direction normal to Γ_b:

$$(22) \qquad \frac{d^2 u_i}{d\xi^2} + \frac{du_i}{d\xi} \;=\; 0 \qquad \forall \eta \in \Gamma_b$$

The solution to (22). subject to the boundary conditions (6). is:

$$u_i(\xi, \eta) = U_b(\eta) - u_o(\xi = 0, \eta)]e^{-\xi}$$
$$(23) \qquad\qquad\qquad \forall \eta \in \Gamma_b$$

and the approximate solution. u_A. is:

$$u_A(\mathbf{x}) = u_o(\mathbf{x}) + [U_b(\eta) - u_o(\xi = 0, \eta)]e^{-\xi}$$
$$(24) \qquad\qquad\qquad \forall \eta \in \Gamma_b$$

In Fig. 1-a we plot a reference solution of (20) obtained by numerical solution of (20) on a very fine grid. In contrast. the results for a coarse numerical solution, u_n, using one spectral element of order $N_x = N_y = 13$. are plotted in Fig. 1-b. The latter solution oscillates throughout the domain. Increasing the number of elements with fixed N_x, N_y leads to smaller wiggles in the solution because of the reduced coupling between the elements as compared with a fully spectral solution. In Fig. 1-c we plot the improved solution u_I obtained using the same coarse grid mesh ($N_x = N_y = 13$) as for the fully spectral solution u_n. The error distribution arising from the fully numerical solution. u_n. and from the different stages of the solution are presented in Fig. 2 a-d. The error of the numerical solution is $||e_n||_\infty = 0.13$ (Fig. 2-a). The error of the present solution after the first analytical correction (obtained on the edge $x = 0$) is still large on the boundary (the edge $y = 0$) on which the correction has not yet been performed (Fig. 2-b). As expected, the error norm after the correction on all boundaries (Fig. 2-c) attains its maximum value near the corners ($||e_a||_\infty = 0.17$). Using the mixed analytical numerical procedure (10) leads to a final solution with error norm $||e_I||_\infty = 4 \cdot 10^{-2}$(Fig. 2-d).

In order to show the efficiency of the present solution, the value of $k = ||e_I||_\infty / ||e_n||_\infty \cdot ||e_A||_\infty$ was estimated for various polynomial degrees and several values of ϵ. The
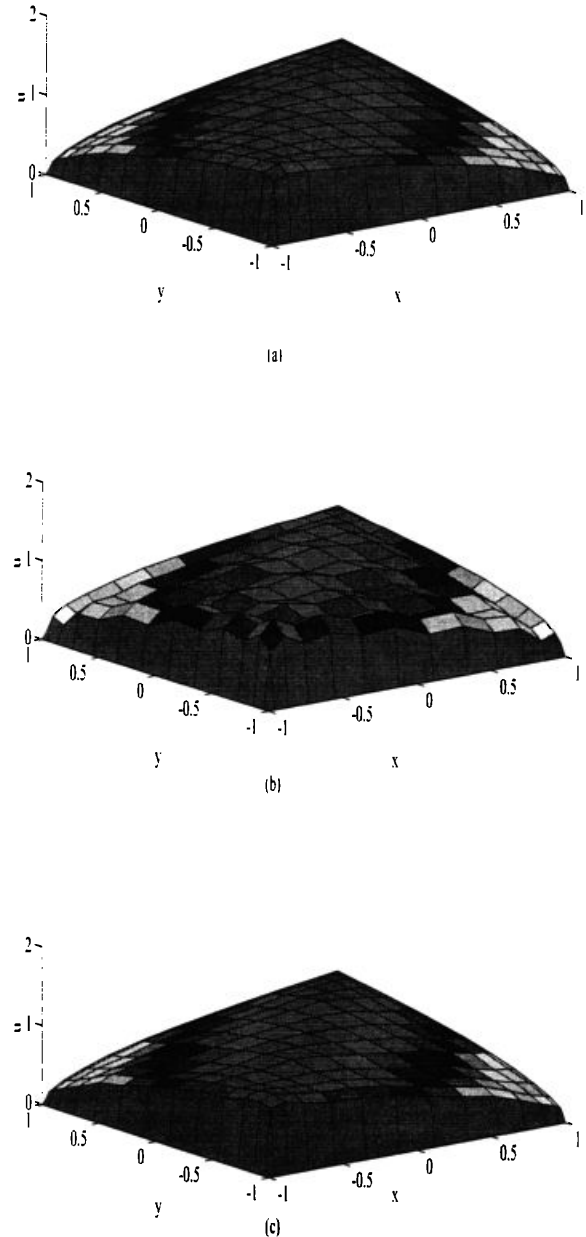
Figure 1: Solution for a two dimensional problem ($\epsilon = 8 \cdot 10^{-3}$). (a) Reference (high resolution) solution (b) Numerical (spectral) solution u_n, $N = 13$ (c) Improved solution u_I, $N = 13$.

(a)

(b)

(c)

(d)
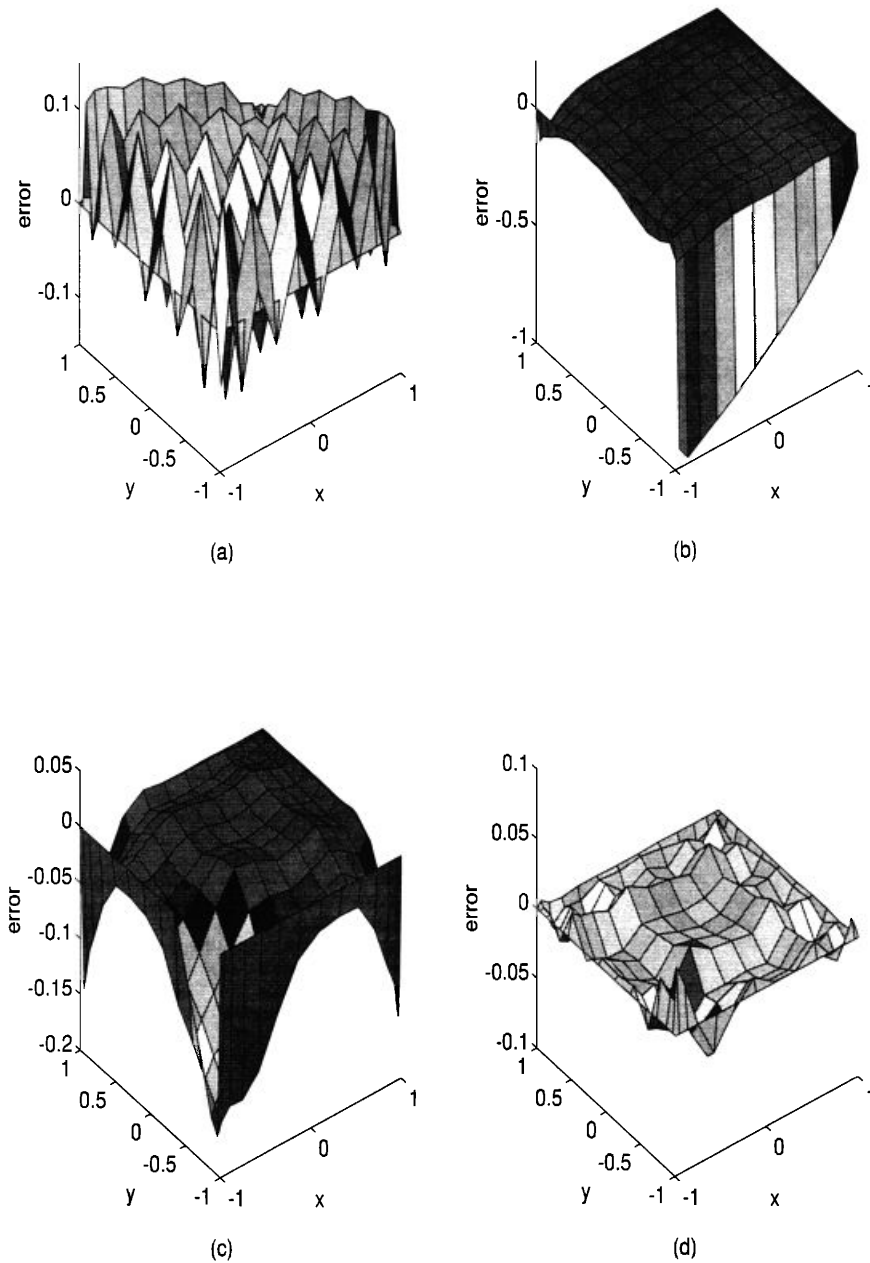
Figure 2: Error distribution ($\epsilon = 8 \ 10^{-3}$). (a) Numerical solution $||e_n||_\infty = 0.13$ (b) First correction$||e||_\infty = 0.97$ (c) Second correction $||e_A||_\infty = 0.17$ (d) Improved solution $||e_I||_\infty = 4 \ 10^{-2}$

boundary conditions were chosen so that an analytical reference solution can be found. The results for k are summarized in Table 1.

For all the values of N and ϵ considered here, k is found to be $O(1)$. For sufficiently small values of ϵ, the method shows an improvement over the fully numerical method. The approximate solution is weakly affected by the polynomial degree of the outer solution since the error e_A is composed of the error of the numerical outer solution and the error of the inner analytical solution, which is dominant.

$N \Downarrow$	$\epsilon \Rightarrow$	0.01	0.008	0.005	0.003
11	$\|e_n\|_\infty$	$3.50\ 10^{-1}$	$5.40\ 10^{-1}$	$1.14\ 10^0$	$2.19\ 10^0$
	$\|e_A\|_\infty$	$3.31\ 10^{-1}$	$1.74\ 10^{-1}$	$8.29\ 10^{-2}$	$3.10\ 10^{-2}$
	$\|e_I\|_\infty$	$3.55\ 10^{-2}$	$2.49\ 10^{-2}$	$2.38\ 10^{-2}$	$1.69\ 10^{-2}$
	k_∞	0.306	0.265	0.251	0.248
14	$\|e_n\|_\infty$	$1.01\ 10^{-1}$	$1.61\ 10^{-1}$	$3.29\ 10^{-1}$	$5.04\ 10^{-1}$
	$\|e_A\|_\infty$	$3.30\ 10^{-1}$	$1.72\ 10^{-1}$	$8.25\ 10^{-2}$	$3.11\ 10^{-2}$
	$\|e_I\|_\infty$	$1.10\ 10^{-2}$	$9.20\ 10^{-3}$	$1.21\ 10^{-2}$	$5.13\ 10^{-3}$
	k_∞	0.33	0.33	0.44	0.32
16	$\|e_n\|_\infty$	$4.80\ 10^{-2}$	$8.80\ 10^{-2}$	$2.20\ 10^{-1}$	$4.00\ 10^{-1}$
	$\|e_A\|_\infty$	$3.1\ 10^{-1}$	$1.74\ 10^{-1}$	$8.22\ 10^{-2}$	$3.09\ 10^{-2}$
	$\|e_I\|_\infty$	$1.80\ 10^{-2}$	$6.43\ 10^{-3}$	$6.15\ 10^{-3}$	$4.8\ 10^{-3}$
	k_∞	1.21	0.42	0.34	0.38
18	$\|e_n\|_\infty$	$2.03\ 10^{-2}$	$6.00\ 10^{-2}$	$1.46\ 10^{-1}$	$3.17\ 10^{-1}$
	$\|e_A\|_\infty$	$3.02\ 10^{-1}$	$1.69\ 10^{-1}$	$8.11\ 10^{-2}$	$2.99\ 10^{-2}$
	$\|e_I\|_\infty$	$1.73\ 10^{-2}$	$5.03\ 10^{-3}$	$3.12\ 10^{-3}$	$2.52\ 10^{-3}$
	k_∞	2.85	0.49	0.26	0.27

Table 1: Comparison between the various stages of the 2-d solution and a numerical solution.

The efficiency of the improved solution compared to a fully numerical solution can be evaluated using the results plotted in Fig. 3. We assume that the number of operations which are needed for a numerical solution is of order of p^3 where p is the total number of degrees of freedom. For $\epsilon = 3\ 10^{-3}$ and $N = 11$ the error obtained from the improved solution is $\|e_I\|_\infty = 1.69\ 10^{-2}$. In order to get a numerical error similar to the error of the improved solution, the polynomial degree of the spectral solution would have to be increased to $N \approx 35$ (see Fig. 3) (even with the highly efficient boundary layer resolution of such a polynomial spectral method). This result means that the ratio between the number of operations for the two solutions is:

$$(25) \qquad eff_{0.003} \approx \left(\frac{35^2}{2\ 11^2}\right)^3 \approx 130$$
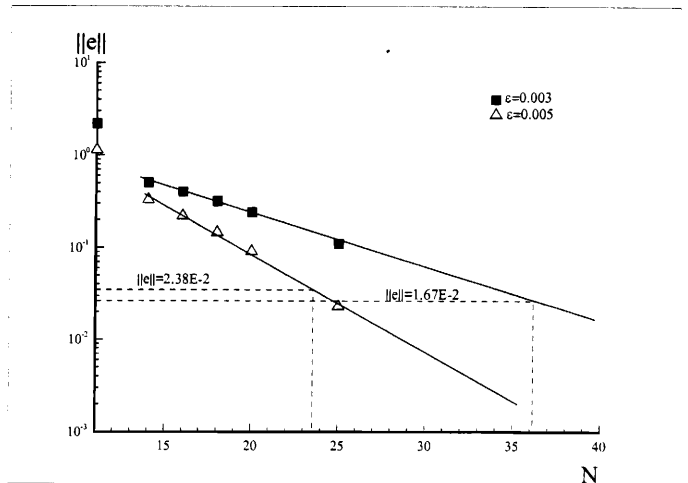
Figure 3: Efficiency of the improved solution.

and for $\epsilon = 0.005$ (see Fig. 3):

$$(26) \qquad eff_{0.005} \approx \left(\frac{25^2}{2\ 11^2}\right)^3 \approx 20$$

The algorithm was also been applied to problems with different values of ϵ in the x and y directions of Ω. If the value of ϵ is high enough in one of the directions the correction could be done only for the second direction in which ϵ is small (see Figs. 4-5). In this case the source of the wiggles is from the x direction so that there is no need to correct the solution in the vicinity of the y boundary.

When $a \neq 0$ in (1) and the velocity of the advection term is parallel to the boundary ($\mathbf{V} = [1, 0]$) two types of boundary layers are present: one of order ϵ and a second one of order $\sqrt{\epsilon}$. In such a case we often need to improve only the solution near the boundary layer of order ϵ. In Fig. 6 we present the results for a test problem: the reference numerical solution is shown in Fig. 6-a. A fully numerical spectral solution based on a low order polynomial approximation (N=13) produces a large oscillatory error because of the x-direction boundary layer $[0(\epsilon)]$. The calculated outer solution, u_0, is presented in Fig. 6-c and is free of oscillations. The hybrid solution can be calculated by matching this solution with a one-dimensional solution, u_i (Fig. 6-d). This solution is much more accurate than the fully numerical solution which is based on the same coarse grid (Figs. 6-e,6-f).

(a)

(b)

(c)
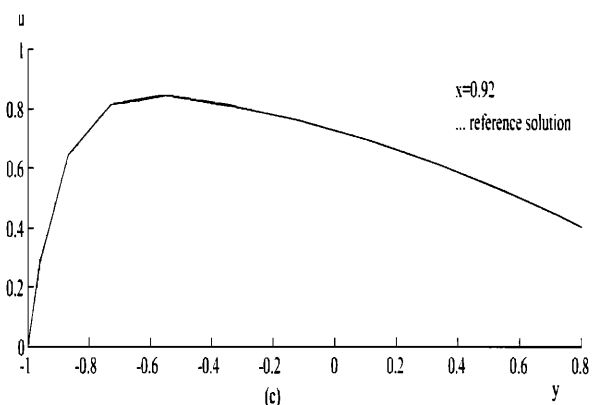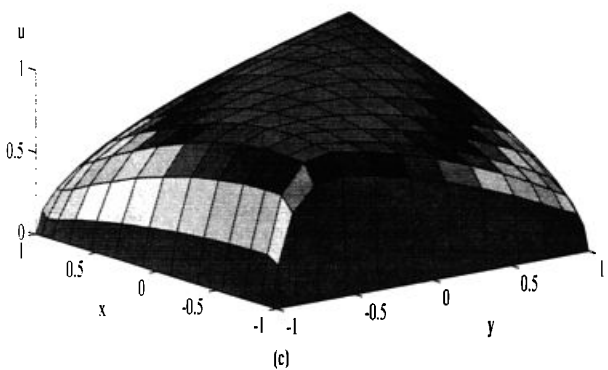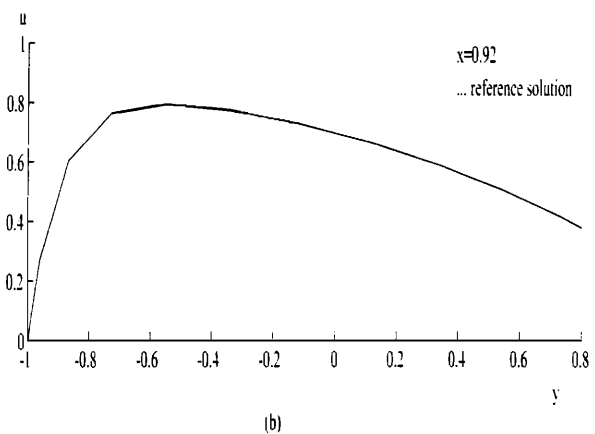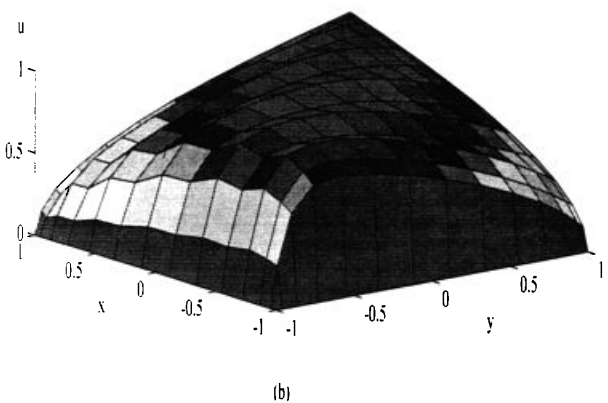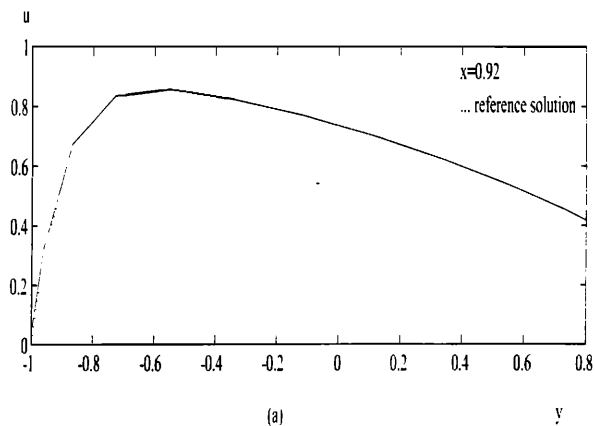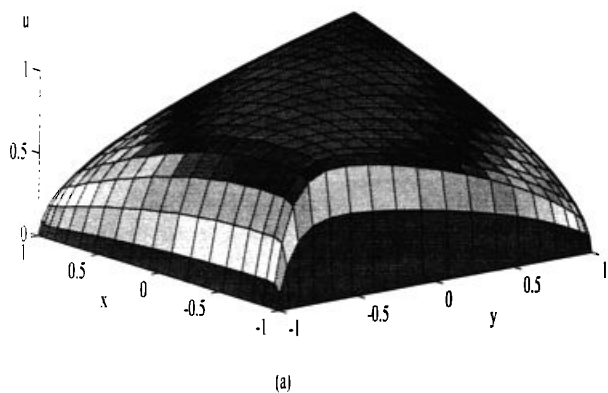
Figure 4: Solution for a two dimensional problem with different values of ϵ ($\epsilon_x = 1 \; 10^{-2}$, $\epsilon_y = 5 \; 10^{-2}$). (a) Reference solution (b) Numerical (spectral) solution u_n, $N = 13$ (c) Improved solution u_I, $N = 13$.

(a)

(b)

(c)

Figure 5: Comparison between various solutions and the reference solution at a fixed x coordinate ($x = 0.92$). (a) Analytical correction $||e_A||_\infty = 0.184$ (b) Numerical solution $||e_n||_\infty = 0.131$ (c) Improved solution $||e_I||_\infty = 4.9 \; 10^{-2}$

7.2 One-dimensional problem with an interior layer

The present algorithm can be applied to the solution of problems having interior layers. To illustrate this, let us consider the following one-dimensional problem:

$$(27) \quad \epsilon^2 u_{xx} - u = -c(x) \qquad x \in (-0.5, 0.5)$$

The outer solution for this equation is calculated numerically as in Sec. 3 and the inner solution, $u_i(\xi)$, should satisfy the equation:

$$(28) \quad \frac{d^2 u_i}{d\xi^2} - u_i = u_o - c \qquad \xi \in [\frac{-x_1}{\epsilon}, \frac{1-x_1}{\epsilon}]$$

where x_1 is the location of the interior layer and $\xi = \frac{x-x_1}{\epsilon}$. For the inner problem it is convenient to use $c(x)$ as an approximation for u_o since the difference between them is of $O(\epsilon)$. The solution for (28) is:

$$(29) \quad \begin{aligned} u_i^{(-)}(\xi) &= Ae^\xi + Be^{-\xi} & \xi \leq 0 \\ u_i^{(+)}(\xi) &= De^\xi + Ee^{-\xi} & \xi \geq 0 \end{aligned}$$

The solutions to both equations should satisfy the conditions that $u_i = 0$ for $\xi \to \infty$ so that :

$$(30) \quad \begin{aligned} u_i^{(-)}(\xi) &= Ae^\xi & \xi \leq 0 \\ u_i^{(+)}(\xi) &= Ee^{-\xi} & \xi \geq 0 \end{aligned}$$

The coefficients A and E are evaluated after applying continuity conditions to both the solution, u_A, and its derivative so that:

$$\begin{aligned} 2A &= u_o^{(+)}(x_t) - u_o^{(-)}(x_t) + \epsilon(\frac{du_o^{(+)}(x_t)}{dx} - \frac{du_o^{(-)}(x_t)}{dx}) \\ 2E &= -u_o^{(+)}(x_t) - u_o^{(-)}(x_t) + \epsilon(\frac{du_o^{(+)}(x_t)}{dx} - \frac{du_o^{(-)}(x_t)}{dx}) \end{aligned}$$
$$(31)$$

As a first example we will consider the case where $c(x)$ is discontinuous at $x_1 = 0.5$:

$$c(x) = \begin{cases} (4x-1)^2 & \text{if } 0 \leq x < 0.5 \\ -(4x-1)^2 & \text{if } 0.5 < x \leq 1 \end{cases}$$

In table 2 we present the maximal error at nodal points for different values of the polynomial degree,N, and ϵ. For the particular differential equation under consideration the numerical solution does not produce wiggles for low values of ϵ(Fig. 6) because it converges to a solution of linear algebraic equations for $\epsilon \to 0$. When the first derivative

$N \Downarrow$	$\epsilon^2 \Rightarrow$	2. 10^{-5}	1. 10^{-5}	5. 10^{-6}	2. 10^{-6}
10	$\|\|e_n\|\|_\infty$	2.97 10^{-2}	2.31 10^{-2}	1.42 10^{-2}	5.93 10^{-3}
	$\|\|e_A\|\|_\infty$	6.40 10^{-4}	3.20 10^{-4}	1.64 10^{-4}	6.40 10^{-5}
	$\|\|e_I\|\|_\infty$	1.29 10^{-5}	9.15 10^{-6}	1.37 10^{-6}	2.39 10^{-7}
	k_∞	0.68	0.67	0.61	0.63
11	$\|\|e_n\|\|_\infty$	2.96 10^{-2}	2.73 10^{-2}	1.86 10^{-2}	8.39 10^{-3}
	$\|\|e_A\|\|_\infty$	6.40 10^{-4}	3.20 10^{-4}	1.64 10^{-4}	6.37 10^{-5}
	$\|\|e_I\|\|_\infty$	1.76 10^{-5}	6.99 10^{-6}	2.20 10^{-6}	4.12 10^{-7}
	k_∞	0.92	0.81	0.74	1.00
13	$\|\|e_n\|\|_\infty$	2.28 10^{-2}	2.96 10^{-2}	2.66 10^{-2}	1.49 10^{-2}
	$\|\|e_A\|\|_\infty$	6.40 10^{-4}	3.20 10^{-4}	1.64 10^{-4}	6.40 10^{-5}
	$\|\|e_I\|\|_\infty$	2.31 10^{-5}	1.29 10^{-5}	4.83 10^{-6}	9.97 10^{-7}
	k_∞	1.50	1.37	1.12	1.04
15	$\|\|e_n\|\|_\infty$	1.35 10^{-2}	2.48 10^{-2}	2.97 10^{-2}	2.22 10^{-2}
	$\|\|e_A\|\|_\infty$	6.40 10^{-4}	3.20 10^{-4}	1.64 10^{-4}	6.40 10^{-5}
	$\|\|e_I\|\|_\infty$	2.85 10^{-5}	1.77 10^{-5}	8.44 10^{-6}	1.72 10^{-6}
	k_∞	3.2	2.26	1.76	1.40

Table 2: Comparison between the various stages of the solution and a numerical solution for discontinuous c(x) .

of u was present in the equation, the numerical solution was less accurate and much more oscillatory (like the two-dimensional boundary layer case). A plot of the different steps of the solution is presented in Fig. 7 for the case $\epsilon = 2 \ 10^{-5}$ and $N = 15$. The inner solution is discontinuous and decays to zero far from the boundary layer. Our final example is the case where $c(x)$ is chosen so that it is continuous within the domain but has a discontinuous derivative at some point within the domain. We choose $c(x) = |x - 0.5|$ so that:

$$(32) \quad u_o^{(-)}(x_t) = u_o^{(+)}(x_t)$$

$$\frac{du_o^{(-)}(x_t)}{dx} = -\frac{du_o^{(+)}(x_t)}{dx} = O(1)$$

For this problem the solution u_A is:

$$(33) \quad u_A = u_o + O(\epsilon)e^{-|\xi|}$$

From Table 3 we can see that for this example the improved solution is much more accurate than both the numerical and analytical approximations. As shown from (27) the numerical and the analytical approximations are of the same order for low values of ϵ. For such problems it may be worthwhile to improve the results by using a
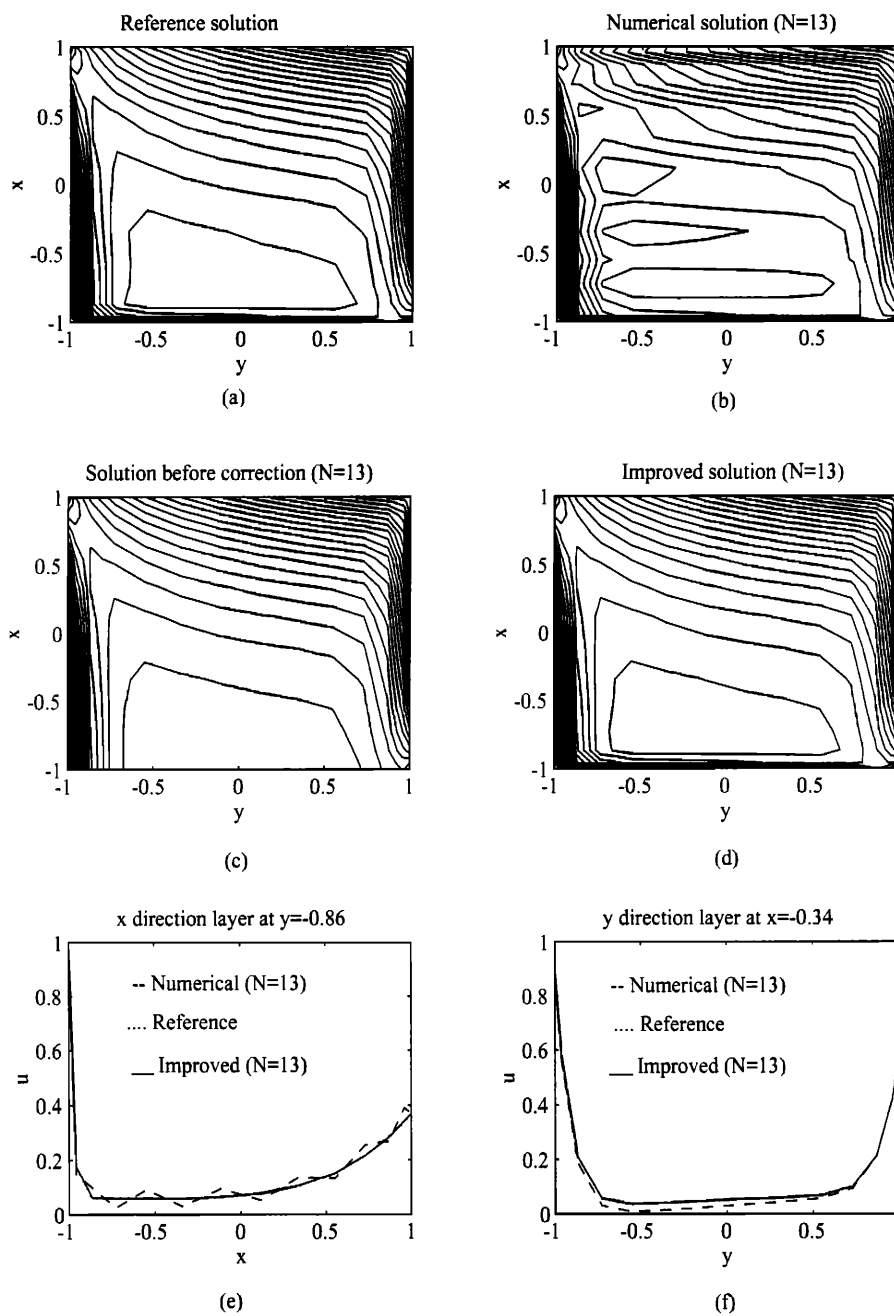
Figure 6: Solution of a two dimensional problem with different types of boundary layer ($\epsilon_x = \epsilon_y = 5 \; 10^{-3}; a = -4; v = [1,0]$). (a) Reference solution. (b) Numerical (spectral) solution u_n, $N = 13$. (c) Outer solution u_o, $N = 13$. (d) Improved solution u_I, $N = 13$. (e) Comparison between the different solutions. in the x direction on a fixed line $y = -0.86$. (f) Comparison between the different solutions in the y direction on a fixed line $x = -0.34$.
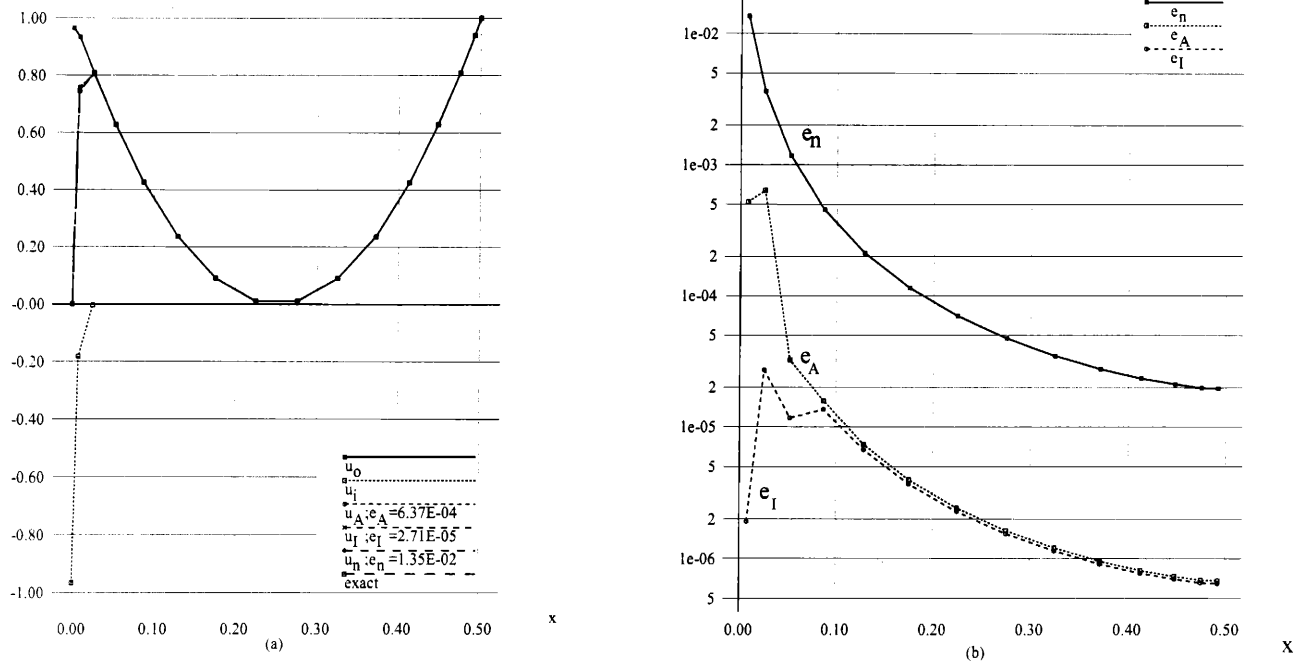
Figure 7: Solution distribution for $0 < x < 0.5$ ($\epsilon = 2 \ 10^{-5}, N = 15$). (a) Different stages of the solution (b) Error distribution

$N \Downarrow$	$\epsilon^2 \Rightarrow$	$1. \ 10^{-5}$	$5. \ 10^{-6}$	$2 \ 10^{-6}$	$1. \ 10^{-6}$	$7. \ 10^{-7}$
11	$\|e_n\|_\infty$	0.399	0.544	0.698	0.783	0.818
	$\|e_A\|_\infty$	0.400	0.345	0.254	0.192	0.165
	$\|e_I\|_\infty$	$8.0 \ 10^{-2}$	$5.9 \ 10^{-2}$	$3.38 \ 10^{-2}$	$2.26 \ 10^{-2}$	$2.24 \ 10^{-2}$
	k_∞	0.5	0.314	0.19	0.15	0.17
12	$\|e_n\|_\infty$	0.317	0.470	0.643	0.742	0.787
	$\|e_A\|_\infty$	0.413	0.377	0.291	0.224	0.193
	$\|e_I\|_\infty$	$8.5 \ 10^{-2}$	$7.23 \ 10^{-2}$	$4.3 \ 10^{-2}$	$3.25 \ 10^{-2}$	$3.28 \ 10^{-2}$
	k_∞	0.65	0.407	0.230	0.196	0.22
14	$\|e_n\|_\infty$	0.182	0.328	0.526	0.651	0.704
	$\|e_A\|_\infty$	0.393	0.412	0.354	0.285	0.250
	$\|e_I\|_\infty$	$7.7 \ 10^{-2}$	$8.5 \ 10^{-2}$	$6.32 \ 10^{-2}$	$6.08 \ 10^{-2}$	$6.36 \ 10^{-2}$
	k_∞	1.07	0.629	0.339	0.32	0.36
18	$\|e_n\|_\infty$	$4.14 \ 10^{-2}$	0.127	0.301	0.454	0.528
	$\|e_A\|_\infty$	0.24	0.356	0.414	0.383	0.353
	$\|e_I\|_\infty$	$2.98 \ 10^{-2}$	$6.33 \ 10^{-2}$	$8.4 \ 10^{-2}$	$7.1 \ 10^{-2}$	$2.56 \ 10^{-2}$
	k_∞	2.95	1.45	0.67	0.4	0.17

Table 3: Comparison between the various stages of the solution and a numerical solution for discontinuous $\frac{dc(x)}{dx}$.

'mixed' numerical solution. Instead of solving for the original differential equation [see (21)] two new variables (u and the derivative of u) can be defined. The correction can then be computed only for the derivative of u.

8 Conclusions

The aim of this work was to present a high-order method that is general and efficient for the solution of multi-dimensional problems with both boundary and interior layers. Our approach exploits the fact that the boundary layer can be treated as a one-dimensional problem to first approximation. In this way the solution is straightforward and does not depend on the dimension of the problem. The calculated solution away from the boundary layer is obtained by using the spectral element method. In this way, the number of degrees of freedom required to obtain the solution is minimal, because the outer solution does not have a boundary layer and thus the spectral convergence is retained. In order to deal with both boundary and interior layers, we used a penalty spectral element method for the numerical solution so that the the outer solution and the corrected solution are calculated on the same grid and there is no need to change the structure of the coefficient matrices. We believe that the new method will be useful for a variety of problems involving interior and boundary layers, including e.g. semiconductor device simulations ([14]).

9 Acknowledgments

References

[1] J. Kevorkian and J.D. Cole. *Perturbation Methods in Applied Mathematics (Applied mathematical sciences; V. 34.* Springer-Verlag, New-York, 1981.

[2] P.A. Markowich. *The Stationary Semiconductor Device equations.* Springer-Verlag, New-York, 1984.

[3] M. Van Dyke. *Perturbation Methods in Fluid Mechanics.* Academic Press, New-York, 1964.

[4] J.J.H. Miller(editor). *Boundary and interior layers : computational and asymptotic methods: proceedings of the BAIL I Conference held at Trinity College, Dublin,3rd- 6th June, 1980.* Boole Press, Dublin,Ireland, 1980.

[5] I. Babuška O.C. Zienkiewicz J. Gago and E.R. Oliveria (eds.). *Accuracy Estimates and Adaptive Refinements in Finite Element Computations.* Wiley, New-York, 1986.

[6] G. Strang and G. Fix. *An Analysis of the finite element method.* Prentice-hall, 1973.

[7] Y. Maday C. Bernardi and A.T. Patera. A new non-conforming approach to domain decomposition: the mortar element method. in H. Brezis and J.L. Lions, editors, *Nonlinear partial Differential Equations and their Applications, College de France Seminar,Pitnman,* 1989.

[8] C. Mavriplis. *Nonconforming Discretizations and a Posteriori error Estimators for Adaptive Spectral Elements Techniques (Ph.D. thesis).* M.I.T, 1989.

[9] J. F. Flaherty and R.E. O'Malley Jr. The numerical solution of boundary value problems for stiff differential equations. *Math. Comp.,31,66-93,* 1977.

[10] M. Israeli and M. Ungarish. Improvement of numerical solutions of boundary value problems by incorporation of asymptotic approximations. *Num. Math., 39:309-324,* 1982.

[11] P. Bar-Yoseph and M. Israeli. An asymptotic finite element method for improvement of solutions of boundary layer problems. *Int. J. for Num. Meth. in Fluids,6:21-34,* 1986.

[12] P. Bar-Yoseph M. Israeli and S. Weichendler. The asymptotic spectral element method. *in 2nd Int. Conf. on Spectral and High Order Methods,* June 22-26, 1989.

[13] A.T. Patera. A spectral element method for fluid dynamics: laminar flow in a channel expansion. *J. Comput. Phys., 54, 468,* 1984.

[14] I. Efrat and M. Israeli. A hybrid solution of the semiconductor device equations. *Proceedings of Nasecode VII,* 1991.